Influence of Austenitization Parameters on the Precipitation Sequence and the Chemical Homogenization of Austenite in a High-Performance Fe–Ni–Cr–Al–Ti–Mo Stainless Maraging Steel

Stella Ancey-Rocchi, Vanessa Vidal, Thibault Poulain, Thomas Billot, Denis Bechet, Nicolas Binot, Vincent Huleux, Moukrane Dehmas, Denis Delagnes

▶ **To cite this version:**

Stella Ancey-Rocchi, Vanessa Vidal, Thibault Poulain, Thomas Billot, Denis Bechet, et al.. Influence of Austenitization Parameters on the Precipitation Sequence and the Chemical Homogenization of Austenite in a High-Performance Fe–Ni–Cr–Al–Ti–Mo Stainless Maraging Steel. Metallurgical and Materials Transactions A, 2021, 52 (10), pp.4623-4635. 10.1007/s11661-021-06415-1 . hal-03328533

HAL Id: hal-03328533

https://imt-mines-albi.hal.science/hal-03328533

Submitted on 6 Sep 2021

HAL is a multi-disciplinary open access archive for the deposit and dissemination of scientific research documents, whether they are published or not. The documents may come from teaching and research institutions in France or abroad, or from public or private research centers.

L'archive ouverte pluridisciplinaire **HAL**, est destinée au dépôt et à la diffusion de documents scientifiques de niveau recherche, publiés ou non, émanant des établissements d'enseignement et de recherche français ou étrangers, des laboratoires publics ou privés.

Influence of Austenitization Parameters on the Precipitation Sequence and the Chemical Homogenization of Austenite in a High-Performance Fe–Ni–Cr–Al–Ti–Mo Stainless Maraging Steel

STELLA ANCEY-ROCCHI, VANESSA VIDAL, THIBAULT POULAIN, THOMAS BILLOT, DENIS BECHET, NICOLAS BINOT, VINCENT HULEUX, MOUKRANE DEHMAS, and DENIS DELAGNES

MLX19 stainless maraging steel grade exhibits a mechanical strength/fracture toughness balance within the required range for landing gear applications. However, the microstructure after the heat treatment still needs to be precisely controlled to obtain a better repeatability of the mechanical properties. This work shows that austenitizing is a critical stage. The influence of austenitization treatment parameters on the microstructure obtained after quenching was thus precisely quantified. It was first revealed that, after a standard austenitization at 850 °C and for specific heating rates and holding times, undissolved β-NiAl precipitates, reaching sizes up to 500 nm, still remain in the as-quenched state, in addition to a high retained austenite fraction. It was also found that large amounts of retained austenite are the result of local heterogeneities in the chemical composition of the austenitic phase prior to quenching, while the undissolved precipitates change the overall chemical composition of the austenitic matrix. New austenitization conditions were thus proposed, leading to a better homogeneity of the chemical composition of the martensitic matrix after quenching.

I. INTRODUCTION

MARAGING steels contain many alloying elements with significant amounts, but are almost carbon-free. Hardening is therefore provided by intermetallic precipitates[1–3] instead of carbides. Nowadays, maraging steels are still at the heart of scientific research, since the ongoing development of new metallurgical solutions makes it possible to obtain the properties required for critical applications.[4]

STELLA ANCEY-ROCCHI is with the Institut Clément Ader (ICA), Université de Toulouse, CNRS, IMT Mines Albi, INSA, ISAE-SUPAERO, UPS, Campus Jarlard, 81013 Albi, France and also with the Aubert & Duval, BP-1, 63770 Les Ancizes-Comps Cedex, France and also with the Safran Landing Systems, 64400 Bidos, France. Contact e-mail: stella.ancey@mines-albi.fr VANESSA VIDAL and DENIS DELAGNES are with the Institut Clément Ader (ICA). THIBAULT POULAIN, DENIS BECHET and VINCENT HULEUX are with the Aubert & Duval. THOMAS BILLOT and NICOLAS BINOT are with the Safran Landing Systems. MOUKRANE DEHMAS is with the CIRIMAT, Université de Toulouse, UPS-INP-CNRS, INP/ENSIACET, 4 allée Emile Monso, BP 44362, 31030 Toulouse Cedex 04, France

Nanometric precipitation into martensite is one of the most effective ways to increase the strength of steels while keeping acceptable levels of ductility. In the 1970s, 250- and 300-type maraging steels were developed and were characterized by a very good balance between mechanical resistance and ductility, thanks to the combined use of a highly strengthening precipitation and a high Ni content for the stabilization of austenite, softer than martensite that promotes the increase in ductility and fracture toughness. Indeed, microsegregations in Ni during ageing lead to the local reversion of martensite into austenite.[5,6] Still in the 1970s, stainless maraging steels designed with addition of Cr emerged. In the 1990/2000s, high-performance stainless maraging steels were developed to further improve both mechanical resistance and fracture toughness (for instance Custom 465[7] and MLX17[8,9] steels), using new combinations of hardening intermetallic phases (often a NiAl and Ni_3Ti combined precipitation) and by controlling the fractions of retained and reverted austenites. After the 2000s, ultra-high-performance stainless maraging steels were developed for challenging applications. The MLX19 stainless maraging steel studied in this paper is a potential candidate for landing gear applications, which require a high mechanical resistance

combined with good fracture toughness and corrosion resistance (UTS ~ 1850 MPa and K_{IC} ~ 50 MPa $\sqrt{m}$).

Heat treatment of MLX19 stainless maraging steel is classically composed of four main stages. First, the austenitization stage, done beyond the AC_3 temperature, aims to obtain an almost fully and homogeneous FCC-austenitic phase. Austenitization is followed by water quenching at room temperature, which leads to a quite soft BCC-martensite with small amounts of retained austenite. According to Ifergane *et al.*,[7] retained austenite can be observed in maraging (or PH-) steels, between the martensite laths. The retained austenite content can be attributed both to mechanical residual compression stresses (caused by the formation of more than 90 pct of martensite during quenching, as described in Reference 10) and to the chemical composition of the high-temperature austenite. In the latter case, as explained in Viswanathan *et al.*,[11] if the austenite chemical composition remains heterogeneous above AC_3, the austenite locally enriched in alloying elements does not transform into martensite during quenching and remains stable up to room temperature. An increase in the amount of retained austenite generally implies a decrease in mechanical resistance, but conversely an increase in ductility, in impact energy (from Charpy test) and in fracture toughness.[10,12] Note, however, that the rapid kinetics of a strain-induced transformation can lead to the transformation of a large amount of retained austenite into martensite with little plastic deformation and thus to a decrease in ductility.[13] Then, MLX19 steel undergoes just after quenching a cryogenic treatment below room temperature, at around -80 °C, to reduce the retained austenite fraction. Finally, the ageing stage, performed at 510 °C during 16 hours followed by air cooling, leads to an intense precipitation of nanometric hardening intermetallic phases into the supersaturated martensite.[14] The first phase to precipitate during ageing is the ordered β-NiAl phase (B2 crystal structure), as it is generally observed in maraging steels containing both Ni and Al.[2,8,9,15–19] These precipitates are generally spherical and nanometer-sized (less than 10 nm). At higher temperatures, the ordered η-$Ni_3(Ti,Al)$ phase ($D0_{24}$ crystal structure) precipitates, as it is often observed for Ti-containing maraging steels.[8,9,15,16,20] These precipitates have generally an elliptical shape and are nanometer-sized too. Finally, ageing also leads to the local reversion of little amounts of martensite into austenite (due to local enrichments in austenite stabilizer elements) below the AC_1 temperature, called reverted austenite,[21–24] which is known to decrease strength and hardness and thus to improve ductility.[25–27] Five different phases, with different sizes (from a few nanometers to several tens of micrometers) are thus coexisting at the end of ageing.

This study focuses on the austenitization stage, which is the last "critical" high-temperature treatment. During the austenitization of massive parts, temperature gradients between the core and the surface of the part can be observed, resulting in a potential microstructural heterogeneity at the end of heating and after quenching. It is therefore essential to understand the effect of heating rate and cooling rate (not addressed in this work), but also of holding time and temperature, on the kinetics of nucleation, dissolution or homogenization of the different phases. Some authors have already focused on this stage in maraging steels. Mondelin,[28] Kapoor and Batra,[29] Viswanathan *et al.*[11] and Carvalho *et al.*[30] studied the austenitization stage regarding the influence of the heating rate on phase transformations. It was clearly established that the amount of precipitates formed during heating decreases as the heating rate increases.[29,30] In addition, the austenitizing parameters (temperature and time) control the retained austenite amounts after quenching, as suggested by References 11 and 31–33. It is stated that chemical composition heterogeneities in the high-temperature austenite lead to larger fractions of retained austenite after quenching.

The main objective of this work is to identify the causes of the variability of the microstructure depending on different austenitization conditions and, in the end, to propose a new heat treatment leading to a more reproducible microstructure (and consequently mechanical properties) after ageing.

II. MATERIAL AND METHODS

A. *Material*

The chemical composition of the investigated MLX19 steel grade (system Fe–Ni–Cr–Al–Ti–Mo) is given in Table I. Ni, Al and Ti alloying elements are involved in the formation of the hardening nanometric precipitates, while Cr and Mo improve stainless properties.[8,9] The alloy was developed by the Aubert & Duval company and was provided, after its thermo-mechanical transformation process, in a thermal state called "as-received state" (state for which the microstructural heterogeneities resulting from steelmaking and processing were almost erased), from which the standard heat treatment can be applied.

The as-received state displays a martensitic-type microstructure with a small amount of retained austenite (between 2.5 and 3 pct). The standard austenitization stage, performed on an industrial scale, consists in a rapid heating at ~ 10 °C/min up to 850 °C, a 1.5 hours holding time and a water quenching. Note that the as-quenched state investigated is a state without cryogenic treatment, in order to precisely analyze the amount of retained austenite after quenching. The estimated average grain size after austenitizing at 850 °C is approximately 60 μm.

To investigate the variability of the microstructure during the industrial austenitization treatment, the influence of three heat treatment parameters was studied: the heating rate and both austenitization temperature and duration. The tracking of the microstructure evolution during the whole austenitization stage was done thanks to *in situ* experiments (dilatometry and high-energy X-ray diffraction (HEXRD)). In addition, the study of the as-quenched microstructure was done thanks to *post mortem* characterizations on samples treated in a laboratory furnace: secondary electron

Table I. Chemical Composition of the MLX19 Stainless Maraging Steel

	Fe	Ni	Cr	Mo	Al	Ti	C
Wt Pct	bal.	12.0	10.0	2.0	1.5	1.2	< 0.02

microscopy (SEM), scanning transmission electron microscopy (STEM), STEM and energy dispersive X-ray spectroscopy (STEM-EDX) and X-ray diffraction (XRD). For both types of experiments, different treatment parameters were used and are detailed in Table II. The cooling rate effect was not studied in this paper and consequently this parameter is fixed for each characterization technique but however depends on the equipment.

Two different austenitization temperatures were considered (850 °C and 950 °C). Prior to the study, the austenite prior grain sizes were estimated for the considered temperatures and heating rates. It was found that the grain size at 850 °C is always equal to about 60 μm (whatever heating rate and holding time), while the grain size at 950 °C evolves during holding between 5 minutes and 2.5 hours, from around 60 μm to maximum 90 μm depending on the heating rate. As an example, the band contrast maps obtained by Electron Backscatter Diffraction (EBSD) analysis are presented in Figure 1 for the samples austenitized at 40 °C/min up to 850 °C and 950 °C for 2.5 hours, cryogenically treated and aged. These band contrast maps reveal the prior austenite grain boundaries and highlight the increase in grain size between 850 °C (~ 60 μm) and 950 °C (~ 80 μm). It is supposed that the size of the prior austenite grains is the same for the as-quenched and aged states.

B. *In Situ Experiments for the Study of Phase Transformations*

Dilatometry experiments were performed on 25 mm long and 3.7 mm diameter cylindrical specimens, initially in the as-received state, in order to reproduce different {Heating→Holding→Cooling} austenitization cycles. Experiments were done on a NETZCH DIL 402C apparatus. Dilatometric signals were systematically corrected thanks to a reference sample in alumina, whose thermal expansion coefficient is well-known.

In situ high-energy (synchrotron) X-ray diffraction (HEXRD) experiments were conducted on the P07 beamline at the Deutsches Elektronen-Synchrotron (DESY) facility in Hamburg (Germany), at the PETRA III storage ring. Figure 2 shows the schematic illustration of the experimental setup used at the DESY facility. Samples were austenitized inside a computer-controlled BAHR DIL 805 A/D dilatometer. Heating was ensured by an induction coil and temperature was measured by a type S thermocouple centrally spot welded on the sample's surface. The high-energy monochromatic beam (λ = 0.124 Å) allowed to work in transmission mode and was associated to a 2D Perkin-Elmer detector permitting diffraction patterns acquisition rates from 0.2 to 10 Hz. The detector was located at ~ 1.5 m from the sample and provided the full Debye-Scherrer rings with a 2θ angle up to 11 deg. Samples (10 mm long cylinders with a diameter of 4.5 mm) were heated under vacuum (< 10^{-4} mbar) and cooled thanks to helium gas at ~ 100 °C/s up to room temperature.

Instrumental parameters of the diffraction setup, like sample-detector distance or beam center, were obtained thanks to LaB_6 standard powder. The conversion of 2D patterns into 1D patterns was done thanks to the FIT2D software. Quantitative analysis was achieved thanks to Rietveld refinement[34] with FullProf package. Then, the evolution of austenite and martensite phase fractions was determined during heating, holding and cooling. Nevertheless, because of its quantification threshold, the Rietveld analysis does not allow to refine the β-NiAl and η-Ni_3(Ti,Al) phases since their phase fractions are very low (~ 1 to 2 pct along complete heat treatment). So for these two phases, only a visual determination of their precipitation and dissolution sequences was directly done on the patterns, degree by degree.

C. *Heat Treatment and Post Mortem Microstructural Characterizations*

Complementary to the *in situ* experiments, the retained austenite phase fraction as well as the microstructure were characterized after the austenitization (into a CARBOLITE - RWF 1200 furnace) and water quenching of parallelepipedic samples of 20 × 20 × 80 mm^3 initially in the as-received state.

STEM observations were performed on polished and electrolytically etched thin foils of 3 mm diameter on the SEM-FEG (FEI Nova NanoSEM 450) microscope equipped with a STEM detector. This equipment was also used for conventional SEM observations.

Table II. Experimental Conditions

Type	Technique	Heating Rate (°C/min)	Temperature (°C)	Time (min)	Cooling Rate
In Situ (See Section II–B)	Dilatometry	1; 3; 10; 40	850; 950; 1000	5 to 150	5 °C/min
	HEXRD	3; 10; 40	850; 950; 1000	5 to 150	100 °C/s
Post Mortem (See Section III–C)	SEM	1	850; 950	5	water quenching (≈ 50 °C/s)
	STEM	1; 40	850	5	water quenching (≈ 50 °C/s)
	STEM-EDX	1; 40	850; 950	5 to 150	water quenching (≈ 50 °C/s)
	XRD	1; 40	850; 950	5 to 150	water quenching (≈ 50 °C/s)

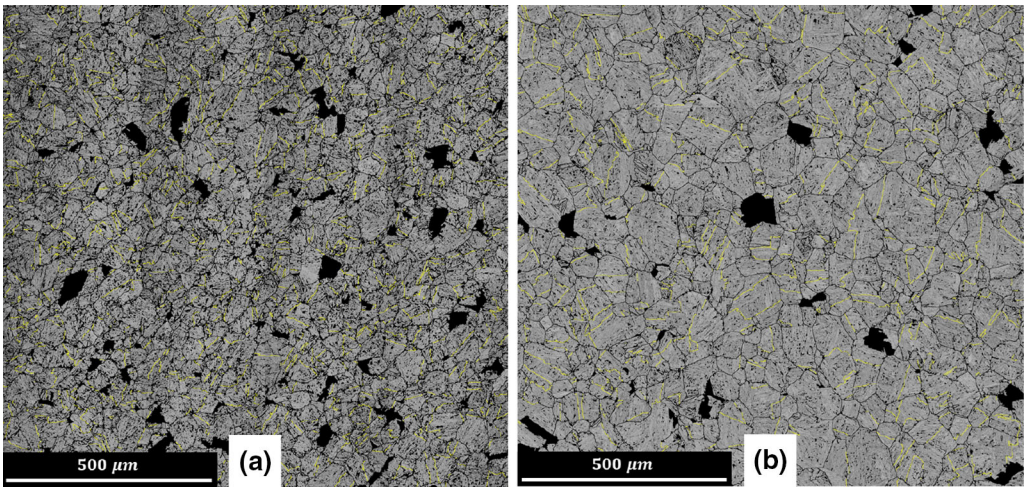

Fig. 1—Band contrast maps obtained after ageing for the samples austenitized at 40 °C/min up to (*a*) 850 °C for 2.5 h and (*b*) 950 °C for 2.5 h. Black areas are areas where reconstruction to austenite was not possible and therefore were not counted for the grain size analysis.

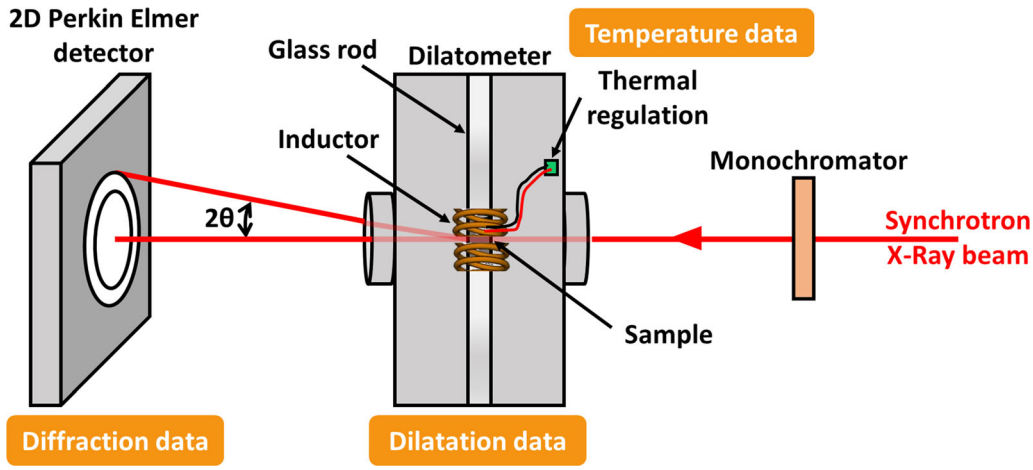

Fig. 2—Schematic illustration of the experimental setup of P07 beamline at DESY.

STEM-EDX maps were done on the same thin foils on a Philips CM20FEG (Bruker EDX silicon drift detector) microscope at the CEMES-CNRS laboratory in Toulouse (France). The chemical elements were quantified through a QMap (Quantitative Element Mapping), which allowed to get rid of thickness variations of the thin foil.

XRD measurements were performed in a Malvern Panalytical X'Pert diffractometer, equipped with a X'celerator linear detector, using Cu-K_α radiation (λ = 1.54 Å).

III. RESULTS AND DISCUSSION

A. *Investigation of Phase Transformations up to 1000 °C by Dilatometry Analysis*

Thanks to dilatometry, austenitization cycles were entirely reproduced. Figures 3(a) and (b), respectively, show the dimensional behavior dL/L_0 (in pct) (where dL is the change in length during heating and L_0 the original length of the sample) and its associated derivative during the austenitization stage of the material for four different heating rates.

Figure 3(a) highlights three different phase transformations, which result in deviations from linearity. These deviations are due either to a decrease in the expansion rate in the case of the precipitation of a new phase within the matrix (lower expansion coefficient for the new phase or depletion in chemical elements in the matrix) or to a matrix volume change, as during allotropic transformations such as the martensite to austenite transformation. Following the conclusions in Reference 8, these three deviations are associated, from the room temperature, to the:

(1) Precipitation of nanometric intermetallic particles β-NiAl into the martensitic matrix,
(2) Precipitation of nanometric intermetallic particles η-Ni_3(Ti,Al) into the martensitic matrix,
(3) Martensite to austenite transformation.

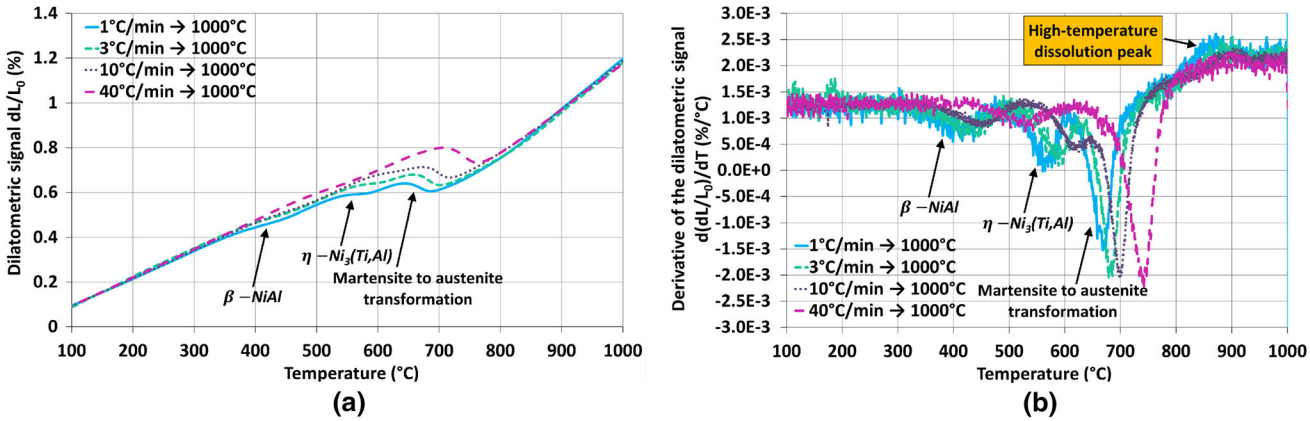

Fig. 3—Dilatometry experiments at the rates of 1, 3, 10 and 40 °C/min. (*a*) dL/L_0 *vs* temperature, (*b*) $d(dL/L_0)/dT$ *vs* temperature.

Figures 3(a) and (b) show that the three transformation temperatures are highly dependent on the heating rate, moving to higher ones when the heating rate increases. This effect was already observed in literature.[11,28–31] For faster heating rates, the time necessary for the diffusion of alloying elements is shorter and the transition temperature is thus shifted to higher temperatures, where diffusion rate is enhanced. The three transformation amplitudes are also affected by the heating rate (Figure 3(b)). When the heating rate increases, the amplitudes of both precipitation peaks decrease. Since some authors[29,30] showed that small precipitation amplitudes correspond to small amounts of precipitates formed during heating, it can be assumed that the lower the heating rate, the more precipitates to form and then to dissolve later.

In addition, a high-temperature dilatation peak is observed for the three heating rates above 850 °C (Figure 3(b)). Its amplitude is all the greater as the heating rate is slow. This peak does not correspond to any identified phase transformation in the MLX19, and the literature does not report such a transformation between 800 °C and 900 °C on similar maraging steel grades. However, given that its amplitude evolves proportionally to the amplitude of the two precipitation peaks, it can be assumed that this peak corresponds to a phase dissolution. A microstructural analysis was therefore conducted to identify the specific transformation leading to this peak at such a high temperature.

B. *Microstructural Observations After Quenching*

Figure 4 shows SEM micrographs of the as-quenched microstructure obtained after austenitization at two different temperatures (850 °C and 950 °C, both for 5 minutes) using the same heating rate of 1 °C/min. After austenitizing at 850 °C for 5 minutes (Figure 4(a)), large amounts of undissolved precipitates (appearing in white on the micrograph), with a size ranging from 100 nm to 1 μm, can be observed. On the contrary, after austenitizing at 950 °C for 5 minutes (Figure 4(b)), no precipitates are detected. According to these microstructural observations, the mechanism associated to the high-temperature dilatation peak detected in dilatometry at around 875 °C for the 1 °C/min heating rate is obviously the dissolution of these precipitates.

In order to compare the size of the undissolved precipitates after slow and fast heating rates, STEM observations were performed on samples austenitized at 1 and 40 °C/min up to 850 °C for 5 minutes. After a slow heating rate up to 850 °C (Figure 5(a)), the undissolved precipitates can be easily distinguished in martensitic matrix (white arrows). Even if some precipitates (not observed here) can occasionally reach a size of 500 nm or even 1 μm according to SEM observations, their size is mainly ranging from 50 to 300 nm. After a fast heating rate up to 850 °C (Figure 5(b)), the undissolved precipitates can still be observed but, as predicted by the dilatometry results, these precipitates are less numerous and are smaller than for a slow heating rate. Indeed, in this case, smaller amounts of precipitates are formed during heating and their growth is then limited to 50 to 100 nm. It can therefore be concluded that a fast heating rate results in the partial bypass of the precipitation process, the martensite to austenite transformation consequently occurring while the martensite is still supersaturated in chemical elements likely to precipitate.

C. *Study of the Precipitation Sequence up to 1000 °C by HEXRD*

To accurately identify the crystallographic structure of these undissolved precipitates, *in situ* HEXRD experiments were performed. Precipitation and dissolution temperatures of both intermetallic phases (ordered β-NiAl and η-$Ni_3(Ti,Al)$) as well as the temperature range of the martensite to austenite transformation were estimated. Heating steps up to 1000 °C with three different heating rates (3, 10 and 40 °C/min) were first carried out. The *in situ* tracking was done visually thanks to the {100}, {200} and {211} peaks for the β-NiAl phase and to the {202} peaks for the η-$Ni_3(Ti,Al)$ phase. The β-NiAl and martensite phases have the same lattice parameter at room temperature but it becomes different with increasing temperature. This phenomenon thus allows to decouple both {200} and {211} peaks of the two phases at high temperature.

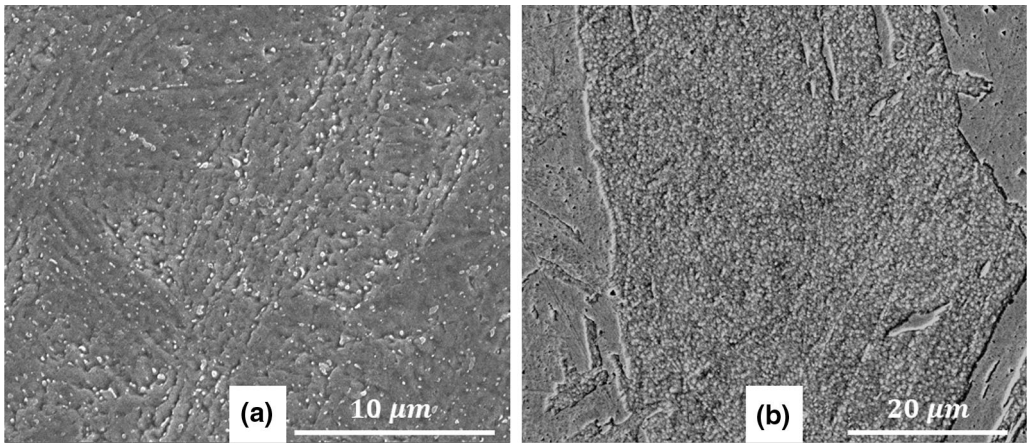

Fig. 4—SEM observation of (*a*) undissolved precipitates in martensitic matrix after quenching the sample austenitized at 1 °C/min up to 850 °C for 5 min and (*b*) martensitic matrix after quenching the sample austenitized at 1 °C/min up to 950 °C for 5 min. The scale is adapted to the grain size.

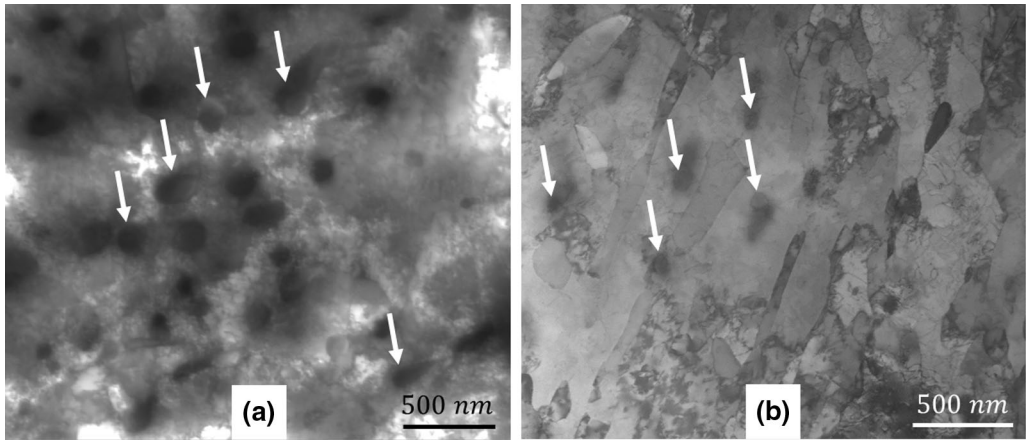

Fig. 5—STEM bright-field images of undissolved precipitates in martensitic matrix after quenching (*a*) the sample austenitized at 1 °C/min up to 850 °C for 5 min and (*b*) the sample austenitized at 40 °C/min up to 850 °C for 5 min.

An example of visual tracking is given in Figure 6 for the heating rate of 3 °C/min, the same procedure being applied for the three heating rates. The criterion adopted for the detection of precipitates is the first identification of a diffraction peak, whereas the complete dissolution is evidenced by the absence of a peak for the concerned phase. The temperature ranges deducted are therefore slightly underestimated, both because of the detection threshold but also the nature of the method which detects a phase only when the crystallographic structure is ordered. For each phase, the peak of maximum intensity has been plotted in red in Figure 6.

The temperatures obtained for precipitates start detection, maximum intensity of the diffraction peaks and complete dissolution for both intermetallic phases are gathered in Table III for each heating rate.

According to these results, η-$Ni_3(Ti,Al)$ precipitates are completely dissolved in the temperature range 690 °C to 740 °C, depending on the heating rate. On the other hand, β-NiAl precipitates are dissolved belatedly: around 900 °C after heating at 3 °C/min and around 915 °C after heating at 10 and 40 °C/min. These dissolution temperatures for the β-NiAl phase perfectly match with the high-temperature dissolution peak revealed by dilatometry experiments. Thus it can be stated that the undissolved precipitates observed by SEM and STEM after quenching from 850 °C belong to the β-NiAl phase. These results provide an explanation for the increase in grain size at 950 °C highlighted earlier. Indeed, the β-NiAl precipitates appear to prevent granular growth at 850 °C whereas, at 950 °C, these precipitates are already dissolved, and the grain growth then becomes dependent on both heating and holding parameters.

D. *Study of the Martensite to Austenite Transformation up to 1000 °C by HEXRD*

In addition to the study of the precipitation sequence, *in situ* HEXRD experiments also allowed to analyze the martensite to austenite transformation. The weight fraction of martensite and austenite phases were quantified by Rietveld refinement between room temperature

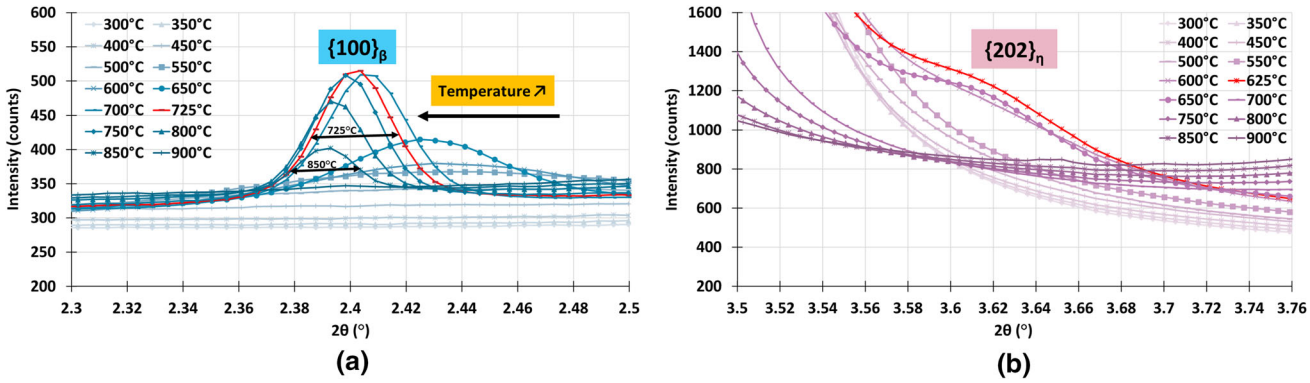

Fig. 6—Evolution of the (*a*) $\{100\}_{\beta}$ and (*b*) $\{202\}_{\eta}$ diffraction peaks every 50 °C between 300 °C and 900 °C during heating at 3 °C/min. FWHM are indicated in figure (*a*) for temperatures of 725 °C and 850 °C.

Table III. Temperature Ranges of β-NiAl and η-$Ni_3(Ti,Al)$ Intermetallic Precipitation During Heating up to 1000 °C at 3, 10 or 40°C/min

	β-NiAl			η-$Ni_3(Ti,Al)$		
Heating Rate (°C/min)	Start Detection (°C)	Maximum Intensity (°C)	Complete Dissolution (°C)	Start Detection (°C)	Maximum Intensity (°C)	Complete Dissolution (°C)
3	400 to 425	725	900	525 to 550	625	690
10	400 to 425	750	915	575 to 600	650	710
40	425 to 450	750	915	625 to 650	675	740

and 1000 °C for the heating rates of 3, 10 and 40 °C/min. The results are plotted in Figure 7 from 400 °C. The temperatures of beginning (austenite weight fraction > 5 pct) and end of the martensite to austenite transformation (austenite weight fraction = 100 pct) are summarized in Table IV. In addition, Figure 7 shows a systematic slope discontinuity observed between 700 °C and 750 °C in the transformation curves for the three heating rates. The associated temperatures are also indicated in Table IV.

When the heating rate increases, the transformation temperatures are shifted to higher values, as already stated by dilatometry experiments. The slope discontinuity occurs at 695 °C, 715 °C and 745 °C for 3, 10 and 40 °C/min heating rates, respectively. While the difference in temperature between 3 and 40 °C/min heating

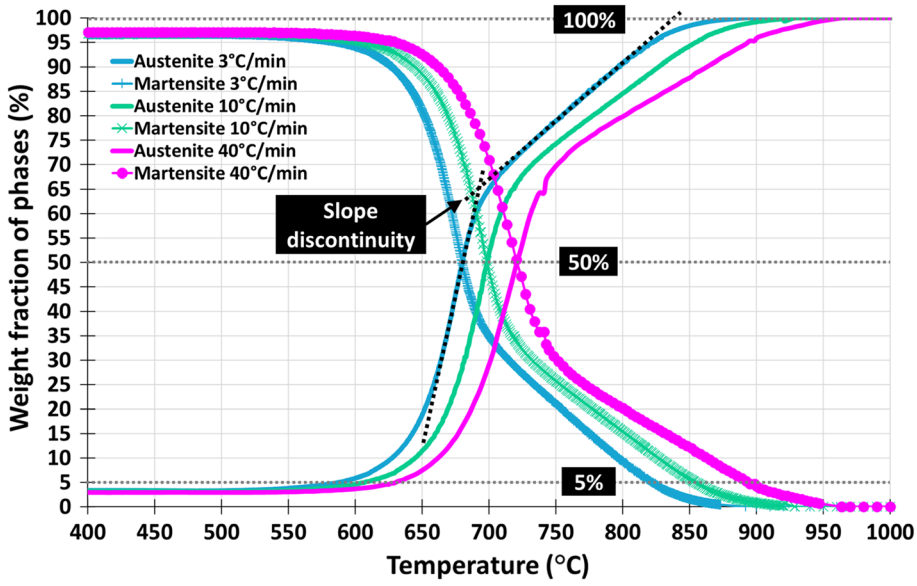

Fig. 7—Evolution of martensite and austenite weight fractions quantified by Rietveld refinement according to temperature between 400 °C and 1000 °C at 3, 10 or 40 °C/min heating rates.

Table IV. Characteristic Temperatures of Martensite to Austenite Transformation During Heating up to 1000 °C at 3, 10 or 40 °C/min

Heating Rate (°C/min)	>5 Pct of Austenite (°C)	Slope Discontinuity (°C)	100 Pct of Austenite (°C)	Transformation Range (°C)
3	590	695	890	300
10	610	715	930	320
40	630	745	965	335
Difference in Temperature (°C) (3 and 40 °C/min)	40	50	75	

Table V. Weight Fraction of Martensite and Approximate Size of Precipitates (When Present) when Reaching 850 °C and 950 °C

	850 °C Without Holding		950°C Without Holding
Heating Rate (°C/min)	Remaining Weight Fraction of Martensite (Pct)	Approx. Size of β-NiAl Precipitates (nm)	Remaining Weight Fraction of Martensite (Pct)
1 to 3	1.6	50 to 300	0
10	5.7	sample not observed	0
40	12	50 to 100	~ 0.6

rates for the beginning of the transformation is about 40 °C, this difference goes up to 50 °C at the slope discontinuity, and up to 75 °C at the end of the martensite to austenite transformation. The increase in this difference therefore means that additional mechanisms after the slope discontinuity accentuate the shift for higher heating rates.

Such a slope discontinuity of the martensite to austenite transformation has already been noticed in literature[35,36] and has been related to the precipitates dissolution by Reference 36. According to Tables III, IV and Figure 7, it can be assumed that the austenite formation starts before the dissolution of both intermetallic phases whatever the heating rate. Afterward, the rapid increase of the austenite fraction in the first part of the transformation can be attributed to the dissolution of the η-Ni_3(Ti,Al) phase, which gradually releases austenite stabilizer Ni in a quite short range of temperature (see Table III) and thus promotes the austenite growth. Indeed, the slope change coincides, to within 5 °C, with the end of the η-Ni_3(Ti,Al) phase dissolution (Tables III and IV). After the slope discontinuity, the maximum intensity of the diffraction peaks is reached for the β-NiAl phase and its dissolution thus begins (both FWHM and intensity decrease, see Figure 6(a)). The decrease in the martensite to austenite transformation rate despite the Ni-rich β-NiAl phase dissolution can be attributed to two factors.

First, when the transformation is almost completed, the growth of austenite is slower and more difficult to achieve because the untransformed martensite resource is low. Indeed, the martensitic phase is detected up to 890 °C after 3 °C/min, and up to 965 °C after 40 °C/min. Note that the presence of martensite at such high temperatures is not usual but has already been evidenced in literature, especially by Christien *et al.*[37] in a 17-4PH stainless maraging steel. Secondly, since the temperature range of the dissolution of the β-NiAl phase is much more extended than for the η-Ni_3(Ti,Al) phase, the Ni enrichment of the martensitic matrix is slower and, consequently, the austenite formation is more progressive. This conclusion is also supported by a faster diffusion of Ni in martensite at such high temperatures (as compared to temperatures corresponding to the η-Ni_3(Ti,Al) dissolution), thus limiting local Ni enrichment around precipitates and consequently preventing the fast transformation into austenite.

The slowing down of the end of the martensite to austenite transformation with the increase in the heating rate can be attributed to martensite homogenization when the β-NiAl phase dissolves. When heating is slow, martensite has time to become chemically homogenized and the transformation of martensite into austenite is gradually promoted. On the contrary, when heating is fast, the time necessary for the diffusion of Ni is shorter and the martensite becomes heterogeneous. Ni-rich zones thus transform easily into austenite, but poor ones do not manage to be destabilized into austenite, which slows down the very end of the austenite formation.

The standard austenitizing cycle performed is currently set at 850 °C for 1.5 hours, with a heating rate of 10 °C/min. With regard to Table V, the temperature of 850 °C without any holding guarantees neither a complete martensite to austenite transformation (remaining fraction of martensite) nor a total dissolution of the β-NiAl precipitates. On the contrary, by reaching 950 °C, the matrix is free from precipitates and fully austenitic, except for the fastest heating rate (less than 0.7 pct of martensite remaining). It is therefore essential to investigate the evolution of the β-NiAl and martensitic phases during holding, particularly at 850 °C.

Table VI. Time Needed to Dissolve the β-NiAl Phase and to Complete the Martensite to Austenite Transformation During Holding at 850 °C and 950 °C After Heating Rates of 3, 10 or 40 °C/min

	850 °C Holding		950 °C Holding
Heating Rate (°C/min)	Time to Dissolve the β-NiAl Phase	Time to Reach a Matrix Containing 100 Pct of Austenite (min)	Time to Reach a Matrix Containing 100 Pct of Austenite
3	> 2.5 h	45	n.d.
10	110 min	50	n.d.
40	65 min	50	< 30 s

n.d. = no detection.

E. *Phase Transformations During Isothermal Holding at 850 °C and 950 °C and the Subsequent Quenching*

To analyze the kinetics of phase dissolution and martensite to austenite transformation during holdings at 850 °C and 950 °C, *in situ* HEXRD experiments were also done. Holding time was set at 2.5 hours for each temperature. Table VI presents the time needed during holding to dissolve the β-NiAl phase and/or to obtain a fully austenitic matrix (no remaining martensite).

Reaching 950 °C, around 0.6 pct of martensite remain at the beginning of holding (Table V), and take less than 30 seconds to finish transforming into austenite. On the contrary, at 850 °C, β-NiAl precipitates are systematically detected, but their dissolution kinetics strongly depend on the heating rate. After a heating rate of 3 °C/min, precipitates are still not dissolved after 2.5 hours at 850 °C. After 10 and 40 °C/min heating rates, the complete dissolution occurs after 110 and 65 minutes, respectively. Thus, fast heating rates before the holding at 850 °C result in the incomplete precipitation of particles (which are also smaller) and therefore in a decrease in the time required for the complete dissolution process. Moreover, at 850 °C, the complete disappearance of the diffraction peaks of martensite is always around 45-50 minutes whatever the heating rate, suggesting that the β-NiAl precipitates remain for several tens of minutes into austenite (from 15 minutes to more than 105 minutes). The chemical homogenization of the austenitic matrix according to the fraction of precipitates being dissolved during holding is therefore an important aspect to control.

Consequently, the evolution of the chemical compositions of the β-NiAl precipitates and the austenitic matrix was estimated using STEM-EDX maps. Experiments were performed on the samples austenitized at 1 °C/min up to 850 °C for 5 minutes and 2.5 hours and at 40 °C/min up to 850 °C and 950 °C for 5 minutes (see Figure 8). Nickel (Ni) element was quantified. After quenching from a 5 minutes holding time at 850 °C (Figures 8(a) and (b)), the undissolved precipitates can be distinctly delimited from the matrix and are located at the martensite laths boundaries. Moreover, a depletion in Ni can be observed around the precipitates (dark bands). This depletion, resulting from the growth stage of the precipitates, seems to be more intense in bands (martensitic laths interfaces or prior austenite grain boundaries) containing several precipitates very close together. The ranges of Ni variations between the Ni-depleted and Ni-enriched bands are about 8 to 15 pct in Figure 8(a) and 4 to 16 pct in Figure 8(b). In the latter case, the Ni heterogeneities are therefore more pronounced. After a 2.5 hours holding time at 850 °C (Figure 8(c)), the matrix is supposed to be nearly homogeneous. Indeed, the Ni-depleted/enriched bands are less visible and the Ni composition varies in the range 9 to 13 pct. Finally, after quenching from 950 °C and despite a fast heating rate and a short holding time (Figure 8(d)), the matrix is almost already homogeneous (Ni variations of 10 to 13 pct).

In addition, the diffusion lengths of Fe, Cr, Ni, Al, Ti and Mo were estimated at thermodynamic equilibrium at 5 minutes and 2.5 hours thanks to the diffusion coefficients calculated by ThermoCalc® with the TTNI8 database and the chemical composition of MLX19 from Table I. Ni is the slowest diffusing element and consequently limits the matrix homogenization before quenching. Its diffusion length is thus compared to the distance between precipitates from one depleted band to another. For a 5 minutes holding time at 850 °C, the Ni diffusion length was calculated to be 45 nm and thus remains well below the mean distance between precipitates, which suggests that the austenitic matrix cannot be fully homogenized. For a 2.5 hours holding time at 850 °C, the calculated diffusion length of Ni reaches 250 nm, which is in the same order of magnitude that the mean distance between precipitates. In this case, the austenitic matrix may remain heterogeneous only when the distance between precipitates exceeds a few hundred nm.

These results show that for a very short holding time, the presence of the β-NiAl phase into the matrix leads to local Ni heterogeneities, limiting the homogenization of the austenitic matrix to a scale of a few hundred nm, especially when the heating rate is fast. The estimated dissolution temperatures thanks to HEXRD also show that for the standard austenitization treatment done at 10 °C/min up to 850 °C, the holding time of 1.5 hours is sufficient to entirely transform martensite into austenite, but not to finish dissolving the remaining β-NiAl precipitates. After a 2.5 hours holding time at 850 °C, the β-NiAl precipitates are still detected but the matrix is much more homogeneous. Finally, at 950 °C, despite fast heating rate and short holding time, the complete chemical homogeneity of austenite has almost been achieved (within the same scale of a few hundred nm).

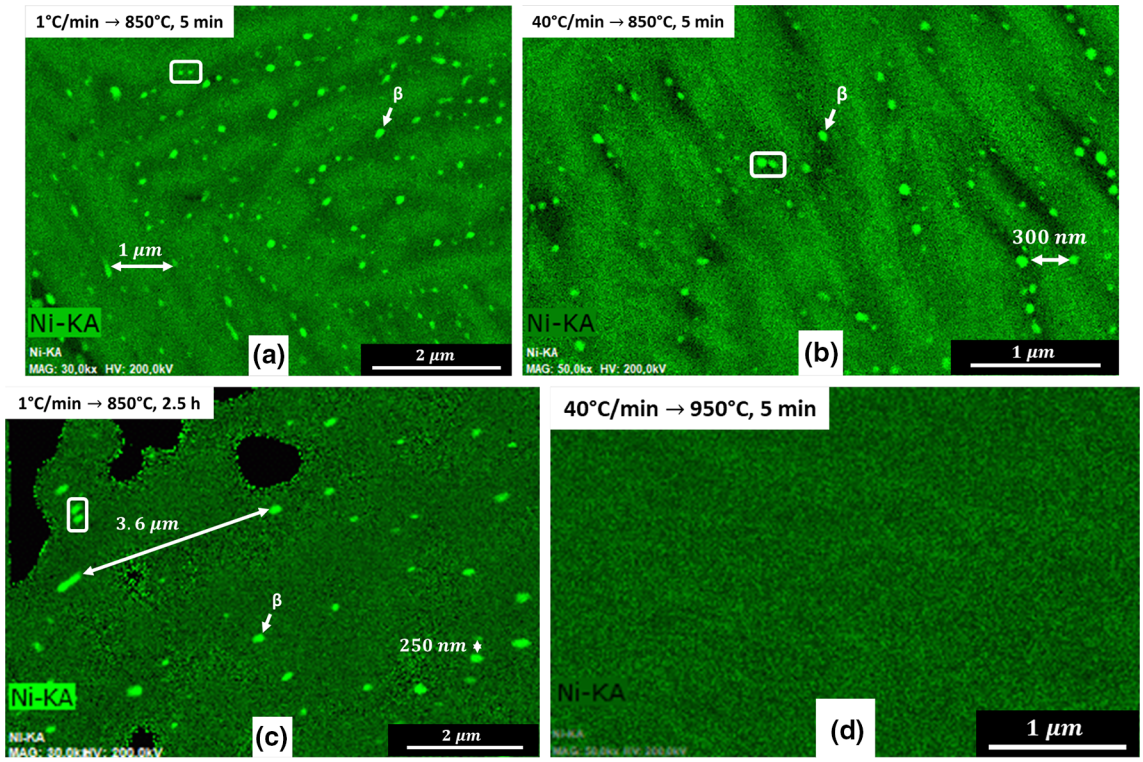

Fig. 8—STEM-EDX maps obtained for Ni element after quenching the samples austenitized at: (*a*) 1 °C/min up to 850 °C for 5 min, (*b*) 40 °C/min up to 850 °C for 5 min, (*c*) 1 °C/min up to 850 °C for 2.5 h and (*d*) 40 °C/min up to 950 °C for 5 min.

The ongoing β-NiAl dissolution change the overall chemical composition of the austenitic matrix and also contributes to local enrichments in Ni into the austenitic matrix before quenching. The retained austenite amounts obtained after quenching as well as the "Martensite starting" (M_s) temperature have therefore been studied for different conditions of heating rate and holding time. In Figure 9 are plotted the M_s temperature and the retained austenite fraction for each investigated austenitization condition.

Since the volume fractions of the β-NiAl phase could not be estimated by HEXRD, image analysis based on the STEM-EDX maps of Figures 8(a) through (c) was performed to quantify the evolution of the β-NiAl surface fraction as a function of the heating rate and the holding time at 850 °C. The results are presented in Figure 10. As predicted by dilatometry and illustrated by STEM, the highest fraction of β-NiAl precipitates (2 pct) is obtained after 5 minutes of holding at 850 °C and for the slowest heating rate. When the heating rate increases and for the same holding time, the fraction obtained is lower. This means that more alloying elements are present in solution in the austenitic matrix. Finally, the lowest surface fraction is obtained for the heating rate of 1 °C/min and the holding time of 2.5 hours. Thus, the β-NiAl precipitates are gradually dissolving during the holding at this temperature and the matrix progressively becomes richer in alloying elements.

Conditions where larger fractions of β-NiAl precipitates remain (*i.e.,* for austenitizations at 850 °C for 5 minutes) are associated with high M_s values, which is in agreement with the literature.[4,26,39,40] Indeed, high M_s temperatures correspond to low amounts of alloying elements in austenite before cooling and thus to very little progress in the dissolution process of the β-NiAl phase, as confirmed by the EDX maps and the associated surface fractions. Since the mean depletion in alloying elements involves mostly the Ni, the austenite is more easily destabilized during cooling and thus transforms into martensite at a higher temperature. As a consequence, the highest M_s temperature (131 °C) is obtained for the sample austenitized at 1 °C/min up to 850 °C for 5 minutes, where the surface fraction of the β-NiAl phase is the highest. When the holding time is increased from 5 minutes to 2.5 hours after heating at 1 °C/min up to 850 °C, the M_s temperature sharply decreases, from 131 °C to 93 °C, due to the ongoing dissolution. The lowest M_s temperatures, whatever heating rate and holding time, are obtained on samples austenitized at 950 °C, where no precipitates remain. After a 2.5 hours holding time at 850 °C and 950 °C, the M_s temperature is quite similar, suggesting that this duration repeatedly leads to a fully austenitic matrix, which has nearly the same chemical composition before the martensitic transformation. As there is no direct link between the range of the Ni variations observed on the STEM-EDX maps and the M_s temperature, it is assumed that the M_s variations are only due to a variation of the average austenite composition as a function of the dissolution progress of the β-NiAl phase. In this regard, Khan and Bhadeshia[41] have shown that

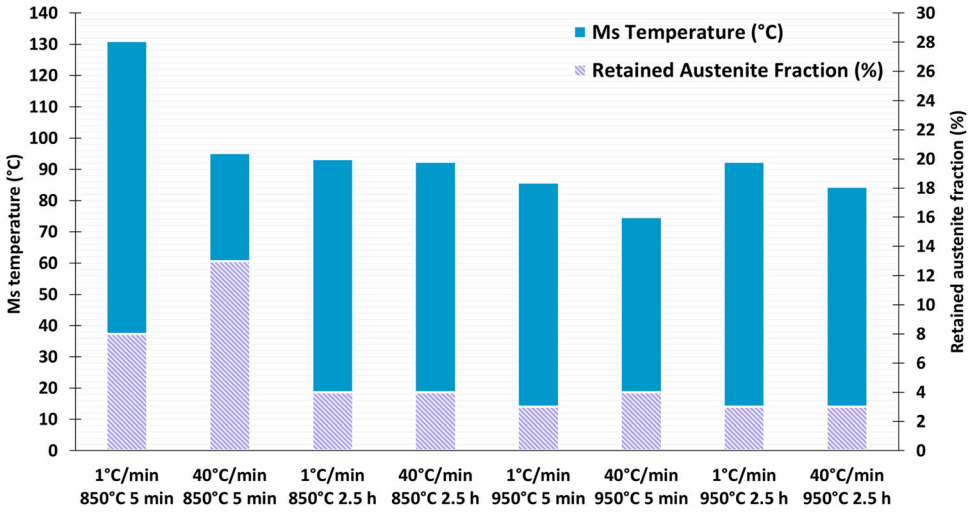

Fig. 9—M_s temperature and retained austenite fraction estimated for different austenitization conditions during a 5 °C/min cooling by dilatometry and after quenching by XRD, respectively. The austenite and martensite phase fractions were quantified in this case using the Reference Intensity Ratio (RIR) method. The RIR method is carefully described in Ref. [38].

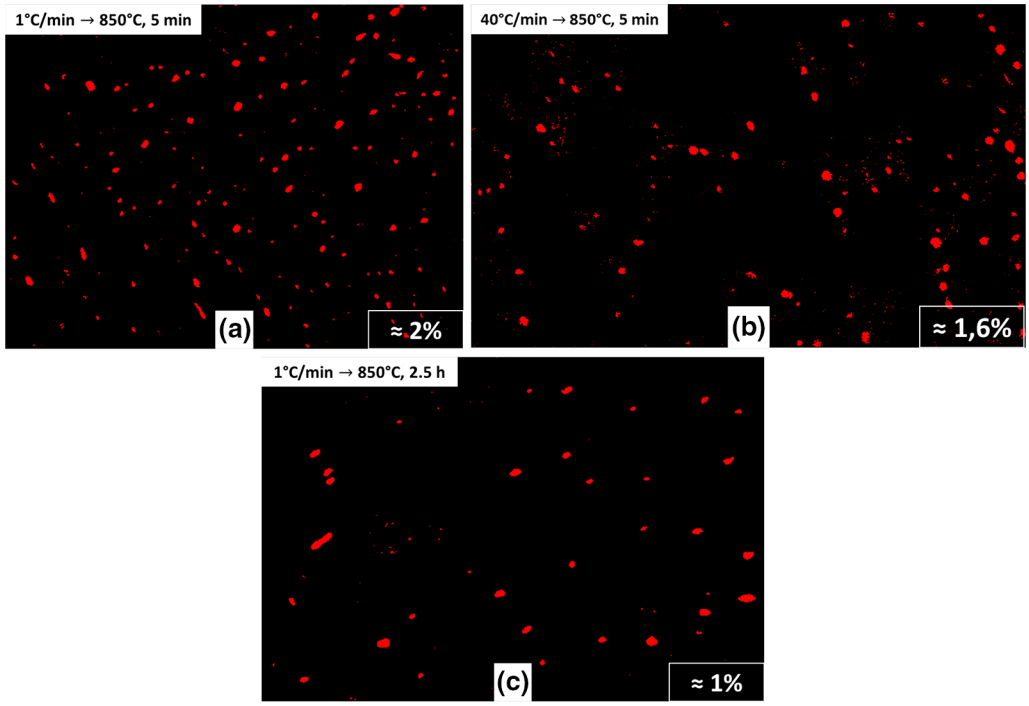

Fig. 10—Image analysis based on the STEM-EDX maps presented in Figs. 8(a) through (c). The β-NiAl precipitates from the thresholding process appear in red and the surface fractions estimated are indicated at the bottom right of each image (Color figure online).

chemical composition heterogeneities before quenching have more influence on the temperature range of the martensitic transformation than on the M_s value. Indeed, the authors describe a chemically heterogeneous sample as a "composite" of different alloys, each having its own range of martensitic transformation.

On the other hand, the retained austenite fractions are directly dependent on the local variations of Ni that are revealed by the STEM-EDX maps. Indeed, as the austenitic phase may be locally too enriched in Ni before quenching to be transformed into martensite,[11,31] the greater the range of Ni variations, the higher the retained austenite fractions. As shown in Figure 9, the largest fraction of retained austenite (13 pct) is obtained on the sample austenitized at 40 °C/min up to 850 °C for 5 minutes. In this case, the high retained austenite amounts after quenching are due to the combination of a high heating rate and precipitates that are still dissolving, which leads to the most pronounced Ni heterogeneities, as shown in Figure 8(b). The second highest retained austenite fraction (8 pct) is obtained on the sample austenitized

at 1 °C/min up to 850 °C for 5 minutes. In this case, the precipitates surface fraction is higher, but the homogenization time of the matrix is longer and the Ni heterogeneities are less pronounced (Figure 8(a)).

Thus, the M_s temperature and the retained austenite fraction provide complementary information on the microstructure at the end of austenitization, just before quenching: while the retained austenite fractions depend on extremely local variations in Ni composition, the M_s temperature depends more on the mean chemical composition of the matrix before quenching. When both M_s temperature and retained austenite fraction have reached their minimum value, the intermetallic precipitates have been totally dissolved and the austenitic matrix has become almost chemically homogeneous.

IV. CONCLUSION

The MLX19 stainless maraging steel was studied during the austenitization stage in order to understand the link between heating and holding parameters and the microstructure obtained after cooling. The different conclusions can be summarized as follows:

1. For austenitizing at 850 °C, the microstructure obtained after cooling strongly depends on the heating kinetics. Indeed, the heating rate will condition in particular the fraction and size of undissolved β-NiAl precipitates at this temperature and consequently the local and global chemical compositions of the austenitic matrix before quenching.
   A fast heating rate at 850 °C, for short holding times, leads to the presence of both martensite not yet transformed into austenite and to undissolved β-NiAl precipitates up to 100 nm in size. After quenching, the retained austenite fractions are high but the M_s temperature is relatively low due to the rather small fraction of undissolved β-NiAl precipitates.
   A slower heating rate leads to a higher surface fraction of β-NiAl precipitates, whose size is also larger than for fast heating rates (up to 300 to 500 nm). The M_s temperature is thus higher. However, due to a better chemical homogenization of austenite before quenching in this case, the fraction of retained austenite obtained after quenching is lower. Based on these results, the as-quenched microstructure is strongly dependent on the duration of the austenitization treatment at 850 °C. It is therefore necessary to control the holding time parameter to obtain a homogeneous chemical composition for the austenitic matrix before quenching.
2. For austenitizing at 950 °C, all the β-NiAl precipitates are already dissolved and the austenitic matrix is almost homogeneous in Ni after 5 minutes, even after a fast heating rate. However, the increase in grain size between 5 minutes and 2.5 hours at this temperature may alter the final mechanical properties and should also be controlled.
3. At the usual heating rate of 10 °C/min, a short holding time at 950 °C or an increased holding time at 850 °C ($>$ 3 to 4 hours) both guarantee the dissolution of the β-NiAl precipitates and the chemical homogeneity of the austenitic matrix. These microstructural conditions before quenching are essential for obtaining an homogeneously distributed and intense nanometric precipitation during ageing as well as a controlled total austenite fraction, likely to reduce the dispersion of the final mechanical properties.

ACKNOWLEDGMENTS

We acknowledge DESY (Hamburg, Germany), a member of the Helmholtz Association HGF, for the provision of experimental facilities. Parts of this research were carried out at PETRA III and we would like to thank Andreas Stark and Norbert Schell for assistance in using P07 beamline. The research leading to this result has been supported by the project CALIPSOplus under the Grant Agreement 730872 from the EU Framework Programme for Research and Innovation HORIZON 2020. Some of the microstructural observations presented in this paper were conducted at the CEMES laboratory and the EBSD analyses were performed at the Centre de microcaractérisation Raimond Castaing, in Toulouse (France). The authors would like to thank Cécile Marcelot for her precious help in the realization of STEM experiments and Arnaud Proietti and Mehdi Salem for their support in the realization of EBSD experiments. Within the Institut Clément Ader laboratory, the authors would also like to thank Sabine Le Roux for her help in the realization of image analysis and Karine Vieillevigne and Serge Tovar for the chemical etchings and the SEM observations.

CONFLICT OF INTEREST

On behalf of all authors, the corresponding author states that there is no conflict of interest.

REFERENCES

1. S. Floreen: *Metall. Rev.*, 1968, vol. 13, pp. 115–28.
2. W. Sha and Z. Guo: *Maraging Steels. Modelling of Microstructure, Properties and Applications*, Woodhead Publishing Limited, Oxford, 2009.
3. W. Sha, H. Leitner, Z. Guo, and W. Xu: *Phase Transformations in Steels—Volume 2: Diffusionless Transformations, High strength Steels, Modelling and Advanced Analytical Techniques*, Woodhead Publishing Limited, Oxford, 2012, pp. 332–62.
4. F. Roch: *Trait. Therm.*, 2008, vol. 390, pp. 51–58.
5. R. Schnitzer, R. Radis, M. Nöhrer, M. Schober, R. Hochfellner, S. Zinner, E. Povoden-Karadeniz, E. Kozeschnik, and H. Leitner: *Mater. Chem. Phys.*, 2010, vol. 122, pp. 138–45.

6. C.H. Beraldo, J.W. Calderón-Hernández, R. Magnabosco, and N. Alonso-Falleiros: *Mater. Res.*, 2019, vol. 22, pp. 1–9.
7. S. Ifergane, M. Pinkas, Z. Barkay, E. Brosh, V. Ezersky, O. Beeri, and N. Eliaz: *Mater. Charact.*, 2017, vol. 127, pp. 129–36.
8. C. Le Nué: *Étude de la relation microstructure/ténacité d'aciers maraging inoxydables*. PhD Thesis. Université de Toulouse, 2017.
9. C. Le Nué, J.M. Cloué, M.H. Mathon, S. Puech, D. Béchet, and D. Delagnes: *Mater. Sci. Forum*, 2016, vol. 879, pp. 413–18.
10. H. Nakagawa and T. Miyazaki: *J. Mater. Sci.*, 1999, vol. 34, pp. 3901–08.
11. U.K. Viswanathan, T.R.G. Kutty, and C. Ganguly: *Metall. Trans. A*, 1993, vol. 24A, pp. 2653–56.
12. M.K. El-Fawkhry, M. Eissa, A. Fathy, and T. Mattar: in *Materials Today: Proceedings*, vol. 2, Elsevier, 2015, pp. S711–14.
13. D. Boussaid: Université de Lorraine, 2018.
14. R. Bhambroo, S. Roychowdhury, V. Kain, and V.S. Raja: *Mater. Sci. Eng. A*, 2013, vol. 568, pp. 127–33.
15. H. Leitner, M. Schober, and R. Schnitzer: *Acta Mater.*, 2010, vol. 58, pp. 1261–69.
16. H. Leitner, R. Schnitzer, M. Schober, and S. Zinner: *Acta Mater.*, 2011, vol. 59, pp. 5012–22.
17. S.D. Erlach, H. Leitner, M. Bischof, H. Clemens, F. Danoix, D. Lemarchand, and I. Siller: *Mater. Sci. Eng. A*, 2006, vol. 429, pp. 96–106.
18. T.H. Simm, L. Sun, D.R. Galvin, E.P. Gilbert, D. Alba Venero, Y. Li, T.L. Martin, P.A.J. Bagot, M.P. Moody, P. Hill, H.K.D.H. Bhadeshia, S. Birosca, M.J. Rawson, and K.M. Perkins: *Mater. Sci. Eng. A*, 2017, vol. 702, pp. 414–24.
19. L. Sun, T.H. Simm, T.L. Martin, S. McAdam, D.R. Galvin, K.M. Perkins, P.A.J. Bagot, M.P. Moody, S.W. Ooi, P. Hill, M.J. Rawson, and H.K.D.H. Bhadeshia: *Acta Mater.*, 2018, vol. 149, pp. 285–301.
20. M. Thuvander, M. Andersson, and K. Stiller: *Ultramicroscopy*, 2013, vol. 132, pp. 265–70.
21. E. Pereloma and D. Edmonds: *Phase Transformations in Steels—Volume 1: Fundamentals and Diffusion-Controlled Transformations*, Woodhead Publishing, Oxford, 2012.
22. W. Sha, H. Leitner, Z. Guo, and W. Xu: *Phase Transformations in Steels—Volume 2: Diffusionless Transformations, High Strength Steels, Modelling and Advanced Analytical Techniques*, Woodhead Publishing, Oxford, 2012.
23. L.T. Shiang and C.M. Wayman: *Metallography*, 1988, vol. 21, pp. 399–423.
24. L.T. Shiang and C.M. Wayman: *Metallography*, 1988, vol. 21, pp. 425–51.
25. J. Bridge and G. Maniar: in *Metallography as a Quality Control Tool*, J.L. McCall and P.M. French, eds., Plenum Press, New York, 1980, pp. 279–95.
26. J.M. Cloué, B. Viguier, and E. Andrieu: *Metall. Mater. Trans. A*, 2005, vol. 36A, pp. 2633–39.
27. R. Schnitzer, S. Zinner, and H. Leitner: *Scr. Mater.*, 2010, vol. 62, pp. 286–89.
28. A. Mondelin, M. Coret, E. Feulvarch, and J. Rech: in *20ème Congrès Français de Mécanique*, 2011, pp. 1–6.
29. R. Kapoor and I.S. Batra: *Mater. Sci. Eng. A*, 2004, vol. 371, pp. 324–34.
30. L.G. de Carvalho, M.S. Andrade, R.L. Plaut, F.M. Souza, and A.F. Padilha: *Mater. Res.*, 2013, vol. 16, pp. 740–44.
31. R. Cozar: *Trait. Therm.*, 1982, (165), pp. 63–71.
32. S. Floreen and R.F. Decker: *Trans. ASM*, 1962, vol. 55, p. 519.
33. H. Hou, H. Li, Y. Jin, X. Wang, and Z. Wen: *Mater. Sci. Eng. A*, 2014, vol. 601, pp. 1–6.
34. H.M. Rietveld: *J. Appl. Crystallogr.*, 1969, vol. 2, pp. 65–71.
35. A. Bénéteau: Université de Lorraine, 2018.
36. W.J. Kaluba, T. Kaluba, and R. Taillard: *Scr. Mater.*, 1999, vol. 41, pp. 1289–93.
37. F. Christien, M.T.F. Telling, and K.S. Knight: *Mater. Charact.*, 2013, vol. 82, pp. 50–57.
38. C.R. Hubbard and R.L. Snyder: *Powder Diffract.*, 1988, vol. 3, pp. 74–77.
39. M. Durand-Charre: *La Microstructure Des Aciers et Des Fontes: Genèse et Interprétation*, Edp Sciences, Les Ulis, 2012.
40. S. da Silva de Souza, P.S. Moreira, and G.L. de Faria: *Mater. Res.*, 2020, vol. 23, pp. 1–9.
41. S.A. Khan and H.K.D. Bhadeshia: *Mater. Sci. Eng. A*, 1990, vol. 129, pp. 257–72.